Published as: Kohn JC, Abdalrahman T, Sack KL, Reinhart-King CA, Franz T. Endothelial cells on the aged subendothelial matrix display heterogeneous strain profiles in silico. Biomech Model Mechanobiol, 2018, DOI: 10.1007/s10237-018-1034-7.

Endothelial cells on an aged subendothelial matrix display heterogeneous strain profiles *in silico*

J.C. Kohn[1,2], T. Abdalrahman[2], K.L. Sack[2], C.A. Reinhart-King[1,3], T. Franz[2,4,*]

[1] Nancy E. and Peter C. Meinig School of Biomedical Engineering, College of Engineering, Cornell University, Ithaca, New York, USA, jck256@cornell.edu

[2] Division of Biomedical Engineering, Department of Human Biology, University of Cape Town, Observatory, South Africa, thomas.franz@uct.ac.za

[3] Department of Biomedical Engineering, School of Engineering, Vanderbilt University, Nashville, Tennessee, USA, cynthia.reinhart-king@vanderbilt.edu

[4] Bioengineering Science Research Group, Engineering Sciences, Faculty of Engineering and the Environment, University of Southampton, Southampton, UK, thomas.franz@uct.ac.za

*Corresponding Author: Dr. Thomas Franz, thomas.franz@uct.ac.za, +27 21-650-1795

ORCID: JCK: none, TA: 0000-0002-0320-811X, KLS: none, CARK: 0000-0001-6959-3914, TF: 0000-0002-1504-3842

Abstract: Within the artery intima, endothelial cells respond to mechanical cues and changes in subendothelial matrix stiffness. Recently, we found that the aging subendothelial matrix stiffens heterogeneously and that stiffness heterogeneities are present on the scale of one cell length. However, the impacts of these complex mechanical micro-heterogeneities on endothelial cells has not been fully understood. Here, we simulate the effects of matrices that mimic young and aged vessels on single and multi-cell endothelial cell models and examine the resulting cell basal strain profiles. Although there are limitations to the model which prohibit the prediction of intracellular strain distributions in alive cells, this model does introduce mechanical complexities to the subendothelial matrix material. More heterogeneous basal strain distributions are present in the single and multi-cell models on the matrix mimicking an aged artery over those exhibited on the young artery. Overall, our data indicate that increased heterogeneous strain profiles in endothelial cells are displayed *in silico* when there is an increased presence of micro-scale arterial mechanical heterogeneities in the matrix.

Keywords: Endothelial cell, cell stretch, finite element model, arterial stiffness, subendothelial matrix, aging

Acknowledgments: The research reported in this publication was supported by the National Research Foundation (NRF) of South Africa (UID 93542), and the South African Medical Research Council (MRC)

under a Self-initiated Research Grant (SIR 328148). Views and opinions expressed are not those of the NRF or MRC but of the authors. Further support was also provided by the National Science Foundation in the United States of America (grant 1738345). J.C. Kohn was supported through the Whitaker International Program.

1. Introduction

Arterial stiffening occurs with advanced age in the artery intima (Huynh et al. 2011; Kohn et al. 2016), the innermost layer composed of the endothelial cell (EC) monolayer and subendothelial matrix. On stiffer substrates, ECs experience decreased cell-cell junction stability, monolayer disruption, and increased permeability (Huynh et al. 2011; Krishnan et al. 2011). Cholesterol permeation into the artery wall is an initiating step in atherosclerosis (Lusis 2000), and the response of ECs to physiological mechanical cues can be disease-promoting. The forces exhibited in the basal layer of cells play a vital role in cellular function; traction forces, arising from actomyosin interactions, are altered by substrate stiffness (Lo et al. 2000), and instability in traction forces is a predictor for endothelial cell-cell junctional gaps (Valent et al. 2016). EC monolayers exhibit more complex mechanics, as cells can detect traction stresses exerted by neighboring cells (Reinhart-King et al. 2008), and forces exerted in one area of an EC monolayer can be transduced across vascular endothelial (VE)-cadherin, a cell-cell junctional protein (Barry et al. 2015). In fact, mechanotransduction mediated through VE-cadherin can trigger signals for focal adhesion and cell-cell junctional disruption (Barry et al. 2015).

Arteries are subject to a combination of mechanical forces during *in vivo* function, including intraluminal pressure, which causes circumferential artery stretch, and axial fluid shear stress due to blood flow (Birukov et al. 1998; Birukov 2009; Sinha et al. 2016). These complex forces can play a role in vascular health, such as through the mediation of vascular smooth muscle cell phenotype (Birukov et al. 1998) and collagen synthesis (Leung et al. 1976) due to cyclic stretch. ECs also respond to stretch by reorganization of the cytoskeleton, where actin filaments align perpendicular to the direction of stretching (Civelekoglu et al. 1998), and through modified signal transduction (Von Offenberg Sweeney et al. 2004) and altered gene expression (Du et al. 1995). Importantly, cyclic stretch also induces nitric oxide production through Akt and endothelial nitric oxide synthase (eNOS) signaling in ECs (Awolesi et al. 1994; Kuebler et al. 2003), and important factor in vascular dilation (Cohen et al. 1999). The combined mechanical forces of cyclic

stretch and shear stress mediate EC orientation, with elongation along the direction of shear stress and perpendicular to substrate stretch (Sinha et al. 2016).

While stiffness micro-heterogeneities occur in the subendothelial matrix (Kohn et al. 2016), and cells are known to respond to complex mechanical cues (Breckenridge et al. 2014), the direct impacts of complex patterns of heterogeneity on ECs are unknown. Previous computational work of cell stretch does not take into consideration the mechanical complexities of the matrix layer (Milner et al. 2012; Mullen et al. 2014). Here, we use computational modeling to simulate the response of a single EC and an EC monolayer to matrix stiffness heterogeneities with the loading conditions of matrix stretch and apical cell shear stress. EC cytoplasmic strains can be measured *in vitro*, and have been measured previously following substrate stretch and fluid shear stress application (Caille et al. 1998; Helmke et al. 2003). Altered intracellular strain distributions provide insight into the effects of exogeneous mechanical forces on cells, and may be influenced by changing cytoskeletal displacements (Helmke et al. 2003). However, the EC cytoplasmic strain patterns resulting from complex stiffness micro-heterogeneities found in *in vivo* arteries have not been elucidated. Here, we find increased heterogeneous basal EC strains when the cell model is placed on a more heterogeneous mechanical profile, representing aged arterial tissue.

2. Materials and Methods

2.1 Animal model and confocal microscopy

All animal treatments and experiments were carried out under Cornell University's Institutional Animal Care and Use Committee guidelines. C57Bl/6 male mice were sacrificed and the thoracic aortas were removed as in our previous study (Kohn et al. 2016). Arteries were cut longitudinally so that the intima could be imaged *en face*. ECs were stained for VE-cadherin with a primary antibody (Santa Cruz, sc-6458) and a secondary Alexa-Flour 488 (Thermo Fisher, A11055). Nuclei were stained with 4',6-diamidino-2-phenylindole (DAPI) (Molecular Probes, D1306). A Zeiss laser-scanning confocal microscope was used to image the tissue, and z-stacks were acquired throughout the entire VE-cadherin layer (Fig. 1a). A representative artery section with aligned endothelial cells was chosen to create the EC monolayer geometry.

2.2 Development of single-cell, multi-cell and matrix geometries

Confocal images were loaded into Simpleware ScanIP software (Synopsis Inc., Mountain View, CA USA) and used to reconstruct the cell geometries. The three distinct cellular components, the cytoplasm, nucleus, and VE-cadherin, were each segmented as separate entities. These segmentations were cropped to achieve a rectangular domain with approximately 15 cells for the multi-cell model. The single and multi-cell geometries are approximately 94 µm and 160 µm long respectively. They both have a thickness of 8-9 µm (measured in the z direction, Fig. 1b). The single cell model was meshed with roughly 17,000 and the multi-cell model with roughly 200,000 C3D4 (4-node linear tetrahedral) elements. The smallest mesh sizes were used which allowed for the model to run in an appropriate time frame and while avoiding mesh clustering around 'pinch points' in the geometries. Finally, in Abaqus 6.14 (Simulia, Dassault Systèmes, Waltham, MA, USA), the subendothelial matrices were created to be 3 µm thick, 500 by 500 µm rectangular prisms and meshed with 30,000 C3D10 (10-node quadradic tetrahedral) elements.

2.3 Material properties

The cell cytoplasm, nuclei, and VE-cadherin were modeled as linear elastic, and their material properties were taken from previous studies, as noted in Table 1. While the multi-cell model includes cell cytoplasm, nuclei and VE-cadherin, the single cell model only includes cell cytoplasm and a nucleus since there are no neighboring cells. The multi-cellular cytoplasm and VE-cadherin were modeled as a single part with different elastic models (using two sets).

Table 1 Material properties of the endothelial cell and subendothelial matrix linear elastic constitutive models. Matrix values are mean ± standard deviation

Material	Elastic Modulus (kPa)	Poisson's ratio	References
Cell Cytoplasm	0.775	0.495	(Caille et al. 2002; Ferko et al. 2007; Yao et al. 2016)
Cell Nuclei	5.1	0.3	(Caille et al. 2002; Ferko et al. 2007; Yao et al. 2016)
VE-cadherin	0.374	0.495	(Barry et al. 2015; Huynh et al. 2011; Nelson et al. 2005)
'Young' subendothelial matrix	24.6 ± 10.6	0.495	(Kohn et al. 2016)
'Aged' subendothelial matrix	30.2 ± 13.6	0.495	(Kohn et al. 2016)

Matrix material properties were based on results from our previous experimental study, where *ex vivo* murine thoracic aortas were probed with atomic force microscopy to determine the spatial profile of micro-scale stiffness of the subendothelial matrix (Kohn et al. 2016). Simulated 'young' (24.6 ± 10.6 kPa) and 'aged' (30.2 ± 13.6 kPa) matrices were created from representative 100 by 100 μm stiffness maps from this previous study (Fig. 1c) (Kohn et al. 2016). The stiffness maps were repeated in a 5 by 5 pattern to span the 500 by 500 μm matrix domain.

2.4 Finite element models

The meshed single-cell and multi-cell geometries were imported and combined with the subendothelial matrices in Abaqus 6.14. To ensure the degrees of freedom at the base of the cell correspond to the deformation experienced on the subendothelial matrix, a node-to-node tie constraint is enforced between the nodes on cell base and the matrix nodes directly beneath the cell (Fig. 1d).

To investigate the effect of 'young' and 'aged' matrix stiffness heterogeneities, the single cell and multi-cell models were placed on 30 and 20 different locations across the matrices, respectively. Due to the process of data acquisition for this study, the cell geometries and the matrix mechanical properties were taken from different mice. Placing the cell models in multiple locations in our computational analysis was used to combat this limitation, as well as provide higher significance to the full width at half maximum comparisons. The elements on the edges of the multi-cell model were removed for strain analysis due to the high boundary strains. Histogram profiles of EC basal strains were created for each location and histogram profiles of mean ± standard error of the mean (SEM) were reported.

Stretch displacement: One edge of the matrix was displaced to induce matrix strain. Other studies using matrix stretch use a range of strain values, from 2 – 25% (Caille et al. 1998; Sinha et al. 2016), providing the effects for different conditions of intraluminal pressure. Given that our model uses subendothelial matrix stiffness profiles from C57Bl/6 thoracic aortas (Kohn et al. 2016), we decided to impose a uniaxial 14.2% displacement on the matrix to mimic the circumferential strain in the mouse aorta of C57Bl/6-background mice (Trachet et al. 2015). The opposite edge of the matrix was fixed in all degrees of freedom, while the two remaining edges were fixed in lateral directions (i.e. only allowed to move in the strained

direction) (Fig. 1d). The free surface of the matrix was fixed in the z direction to ensure the EC(s) only experience in-plane motion.

Shear load: To simulate fluid shear stress over the EC(s) due to blood flow, a traction of 12 dyn/cm^2, as used in our previous shear experiments (Kohn et al. 2015), was placed on the apical surface of the cell(s) in a direction parallel to the long axis of the cell (Fig. 1d). Shear load was used in all of the models, although its effects on the cell basal strains were negligible (data not shown).

Fig. 1 Single and multi-cell models were created from confocal images and loaded by matrix deformation and shear stress. (a) *Ex vivo* murine confocal images stained for VE-cadherin and nuclei were used to create (b) single and multi-cell geometries. (c) Atomic force microscopy data from our previous experimental study (Kohn et al. 2016) were used to create maps of matrix stiffness heterogeneities, demonstrating the complex stiffness patterns found *in vivo*. (d) The cell models were tied to the center of the matrix. The matrix was stretched perpendicular to the direction of cell elongation and shear was applied parallel to cell elongation on the apical surface. Boundary conditions were set so displacement occurs only in the x-direction

2.5 Data and statistical analysis

Maximum principal logarithmic strain and von Mises stress values from the matrices and EC(s) at integration points of each element were exported from Abaqus. Prism 7 software (GraphPad Software, San Diego, CA, USA) was used to plot the data and perform statistical analysis. To assess heterogeneity, Gaussian distributions were fit to histograms of stress and strain of the young and aged matrices and the strain values at multiple locations of the cell(s) on the matrix, using Prism software. Full width at half maximum (FWHM) values were calculated from the standard deviations of the Gaussian curves (Weisstein) as:

$$FWHM = 2\sqrt{2\ln(2)} * standard\ deviation$$

Data were assessed for normality using the Shapiro-Wilk normality test and parametric data were analyzed by Student's t-test between two groups. Percent difference between the means was calculated

as the difference in means over the average in the means and expressed as a percentage. Error bars are presented as SEM unless otherwise noted.

3. Results

3.1 Effect of matrix stiffness heterogeneities on matrix stress and strain

Representative aged matrix exhibits increased heterogeneity compared to the young matrix

Matrices mimicking young and aged murine subendothelial matrix stiffness patterns underwent a 14.2% physiological stretch on one side. After deformation, the matrices displayed complex patterns of strain heterogeneity where both matrices displayed different 'hotspot' regions of high strain values (Fig. 2a). After deformation, the aged matrix also displayed more regions of high stress compared to the young matrix (Fig. 2b).

Fig. 2 Matrices representing young and aged murine vessels display complex strain and stress patterns after stretch. The profiles of (a) strain and (b) stress in the stretched matrices indicate complex patterns of heterogeneity, with different 'hotspot' regions in the matrices. Zoomed in plots of the repeated patterns demonstrate the large differences between the two matrix profiles and more high stress regions in the aged matrix

Data were collected from the matrix strain and stress profiles for both young and aged matrices. Histogram plots of matrix strains and stresses (Figs. 3a, b) were fit to Gaussian curves (Figs. 3c, d). While the mean strains are similar for both matrices, the mean stresses shift rightward towards higher values in the aged matrix due to the higher stiffness values. Full width at half maximum (FWHM) values were calculated from the Gaussian distributions and serve as a measure of heterogeneity. The aged matrix was found to exhibit higher FWHM values for both matrix strain (young: 0.065; aged: 0.086) and stress (young: 2402; aged: 2852). These data indicate that the aged matrix exhibits more heterogeneous strain and stress profiles.

Fig. 3 Aged matrix strain and stress patterns exhibit increased heterogeneity. (a) Histogram profiles of matrix strain and (b) stress were plotted from the young and aged matrices. (c, d) Histogram profiles were

fit with Gaussian curves, showing the spread of values and the rightward shift in matrix stress in the aged matrix. Full width at half maximum (FWHM) values were calculated from the Gaussian distributions as indicated by the arrows; FWHM values are higher in the aged matrix, for both matrix strain (young: 0.065; aged: 0.086) and stress (young: 2402; aged: 2852)

3.2 Effect of matrix stiffness heterogeneities on endothelial cell(s)

3.2.1 Endothelial cells display more heterogeneous basal strains on an aged matrix

Cell strains in the basal plane are reported in this study to assess the area that is the most impacted by the matrix heterogeneities. In the single cell model, complex intracellular strain patterns indicate that when the cell is placed on the aged matrix, more regions of high and low cell basal strain are displayed than when the cell is placed on the young matrix (Fig. 4a). The multi-cell model was cropped to account for the high strains at the boundaries, and these strain contours also demonstrate increased numbers of high and low strain 'hotspots' in the cell monolayer when it is placed on the aged matrix compared to the young matrix (Fig. 4b). The complex strain profiles exhibited by the cell models indicate that the cells respond to micro-scale stiffness profiles present in the matrices.

Fig. 4 Strain patterns in the single and multi-cell models are affected by matrix stiffness heterogeneities. (a) Basal strains in a representative single cell display more high and low strain 'hotspots' in the cell when placed on the aged matrix (indicated by arrows). (b) 'Hotspot' regions of high and low strain are exhibited in a representative multi-cell model (indicated by arrows), where more occur on the aged matrix. These complex cell strain profiles demonstrate that the cells react to micro-scale changes in matrix stiffness

The single and multi-cell models were placed in 20 – 30 different locations on the young and aged matrices, and the basal cell cytoplasm strain values were recorded in each location and averaged to create histogram plots. Mean histogram plots demonstrate the increased heterogeneity of basal cell strains when the cell models are placed on the aged matrix (Figs. 5a, b). Gaussian curves were fit to the histograms (Figs. 5c, d), and heterogeneity was quantified using FWHM, demonstrating increased heterogeneity in EC basal strains on the aged matrix for both models (Fig. 5e). These data indicate that micro-stiffness heterogeneities present *in vivo*, such as in the aged matrix model, induce more heterogeneous basal cell strains.

Fig. 5 Basal cell strains increase in heterogeneity on an aged matrix. The mean histogram plots of (A) single and (B) multi-cell basal cytoplasm strains display increased heterogeneity when the cell models are placed on the aged matrix; error bars are SEM. Gaussian distributions of mean histograms for the (C) single cell model and (D) multi-cell model demonstrate the spread of values using full width at half maximum (FWHM), represented by the arrows. (E) Histogram data is represented as mean plots of 30 different matrix locations for the single cell model and 20 different locations for the multi-cell model. Heterogeneity is quantified by FWHM after histograms were fit to Gaussian distributions, and indicate increased basal cell strain heterogeneity for both cell models placed on the aged matrix. *** $p < 0.0005$, Student's t-test

3.2.2 Local matrix stiffness inversely correlates with local cell strain

A representative region with high heterogeneity was selected to demonstrate the local effects of matrix stiffness heterogeneities on ECs. Regions of compliant matrix stiffness result in relative increases in matrix strain at these region; regions of high matrix stiffness result in decreased matrix strain (Fig. 6a). These localized heterogeneous matrix strains correlate with the single cell basal strains at the respective locations (Fig. 6b). The same effect, although more muted, is found for the multi-cell model when placed on the same heterogeneous matrix region (see the corresponding areas in the pink and black circles) (Fig. 6c). Overall, these data demonstrate that micro-stiffness heterogeneities in the matrix influence the local strain distributions in ECs.

Fig. 6 Micro-scale stiffness heterogeneities present in the matrix cause local heterogeneous cell basal strain. (a) A heterogeneous subendothelial matrix stiffness region from a previous study (Kohn et al. 2016) was chosen. The area of increased matrix stiffness (outlined in the pink circle), induces decreased matrix strain. The area of low matrix stiffness (outlined in the black circle) induces increased matrix strain and more local x deformation. (b) The single cell model was placed on this region of high stiffness heterogeneity, and in the region of high stiffness, the local matrix and cell strain decreased (pink circle). The region of matrix compliance induces opposite strain profiles (black circle). (c) The multi-cell model was placed in the same matrix location, and demonstrated the same strain patterns as the single cell model

3.2.3 The same cell geometry in the single or multi-cell models displays similar strain profiles

As the single and multi-cell geometries were developed from the same confocal image data, the same cell is present in both models. As seen in Fig. 6, both models were placed on a matrix region with high stiffness heterogeneity, and the local basal strains were examined. When fixed to the same corresponding subendothelial matrix region, cell geometries from the single and multi-cell models demonstrate similar regions of high and low cell strain (Figs. 7a, b). In this analysis, only basal cytoplasm values were used, and the slight geometrical differences in the cell is due to the addition of VE-cadherin in the multi-cell model. Between the two models, cell basal strains display a similar range of values; the mean basal strains demonstrate a 12.2% difference between the same cell in both models (Fig. 7c). These data indicate that the single and multi-cell models result in similar cell strain outputs. Furthermore, matrix stiffness is the dominant influence on the deformation of a cell and its resulting basal strain profile.

Fig. 7 The same cell geometry used in the single or multi-cell model demonstrates similar basal strain profiles. (a) The single cell model basal strain contour plot demonstrates regions of high and low strain, as in Fig. 6b. (b) The center cell from the multi-cell model, the same geometry as used in the single cell model, can be used to compare cell strains between the models. The strain profiles throughout the cell indicate similar regions of high and low values in both models. (c) For the same cell geometry in both models, the mean strain differences between the single and multi-cell models differ by only 12.2%, indicating that the two models predict similar basal cell strain patterns

4. Discussion

Here, we demonstrate a computational model of endothelial cell strain patterns on a matrix with heterogeneous mechanical properties. Previously, the artery has been shown to increase in heterogeneous stiffness with age (Graham et al. 2011), and this specifically occurs in the subendothelial matrix (Kohn et al. 2016). Recently, stem cells have been demonstrated to respond to heterogeneous matrix cues by displaying heterogeneous traction forces (Breckenridge et al. 2014). However, the effects of complex patterns of stiffness micro-heterogeneities on ECs had not been elucidated. Previous computational studies of cell stretch do not take into account the mechanical heterogeneities of the matrix (Milner et al. 2012; Mullen et al. 2014); here, we added heterogenous complexity to the matrix to create a more physiologically representative model. Our main finding is that ECs placed on an aged

subendothelial matrix *in silico* display increased EC strain heterogeneity. Complex cytoplasmic strain distributions caused by exogeneous mechanical cues can be altered via cytoskeletal displacement (Helmke et al. 2003), and therefore serve as a useful intracellular metric. This computational model, which incorporates complex mechanical matrix properties, is a starting point for the assessment of EC mechanical responses and possible phenotypic changes to complex physiological stiffness profiles.

Our results indicate a close connection between localized matrix stiffness and localized EC strain, which is most apparent in cells on high-heterogeneity regions. Previously, experimental analysis of ECs after uniaxial substrate stretch indicated that the cell cytoskeletal strains closely follow the deformation of the substrate (Caille et al. 1998). Strain has also been experimentally shown to be transferred into cellular cytoplasm from a stretched substrate with a strain transfer ratio of 0.79 (Gilchrist et al. 2007). Here, we expand on this knowledge by assessing the cellular impact of heterogeneous matrix stiffness computationally and demonstrate the effects of localized stiff matrix regions. Moreover, we indicate that intracellular strains in the multi-cell model are similar to those in the single cell model, indicating that the effects of complex patterns of matrix deformation may also affect cells in larger cell monolayers. Differences between these models may be accounted for based on the more complex geometry of the multi-cell model as well as the inclusion of VE-cadherin in this model. However, cell strain values obtained with both models demonstrate cell strains on micro-scale regions of high or low matrix stiffness.

Our data indicate that *in silico* cell strain, transferred through matrix stretch into the EC, can be affected by matrix stiffness in localized regions. However, the possible implications of these intracellular strain profiles on vascular function have not been determined. Interestingly, a recent study by Dan et al. (2016) revealed that substrate stiffness and cyclic stretch in concert mediate EC monolayer disruption to thrombin-induced barrier disruption (Dan et al. 2016). In this study, ECs plated on 15 kPa hydrogels also exhibited larger cell-cell gaps than those on 5 kPa gels, but this effect was attenuated by cyclic strain application. While EC barrier integrity is known to be mediated by substrate stiffness-dependent actomyosin contractility (Huynh et al. 2011; Krishnan et al. 2011), and now by stiffness and cyclic stretch in concert (Dan et al. 2016), the effects of complex heterogeneous patterns of stiffness remains unknown. Future studies should examine the effects of local regions of stiffness heterogeneity on monolayer function and barrier integrity.

This computational model is derived from *ex vivo* tissue analysis, used to obtain cell geometries and the stiffness profiles of the representative matrices. Given the nature of these data collection, it was not possible to obtain these data from the same location, and therefore the cell geometries do not reflect the exact conformations of the cells on the representative matrices used. Since there is no spatial link between the orientations of the cell and the subendothelial matrix models, our computational findings cannot accurately predict the effects of the spatial heterogeneities in alive endothelial cells. In future studies, the model should take into account the cell-to-matrix spatial orientations. In addition, due to the manual input each matrix mechanical value, we used a repeated 100 by 100 µm matrix to create the larger 500 by 500 µm matrix for the study. While this method still does mimic *ex vivo* tissue properties, repeating the pattern was a necessary compromise to the work. Another limitation of our study is the flat interface used between the cell and matrix, which does not mimic the focal adhesion contacts observed experimentally. However, in previous computational models, focal adhesions were also not considered as discrete elements with specific geometry and mechanical properties. Mullen *et al*. (2014) considers the contact between the cell and substrate through selected areas in the bottom surface of the cell and refers to these areas as focal adhesions (Mullen et al. 2014). Slomka and Gefen (2010) assumed a tie constraint between the cell base and elastic plate to represent focal adhesions which effectively resist tension applied to the cell (Slomka and Gefen 2010). Another computational model by Milner et al. (2012), analyzed cell strains after stretch using a uniform cell-matrix interface. In fact, uniform contact models can be an appropriate comparison for some *in vitro* cell stretch studies (Schaffer et al. 1994; Caille et al. 1998; Park et al. 2004). In this article we used tie constraints throughout the basal cell layer and the underlying matrix. Given that our model assumption of a flat cell-to-matrix interface does not represent physiological conditions, in the future, this model should incorporate focal adhesion contacts between the cell and matrix. While interesting hypotheses could be tested in a model including discrete focal adhesions, this was beyond the scope of our study.

5. Conclusions

To assess the impact of matrix stiffness heterogeneities on endothelial cell strain, computational models were created of single and multiple endothelial cells on matrices with different patterns of stiffness heterogeneities. The cell models were placed on a representative ‘young’ and ‘aged’ matrices, which displayed different levels of strain heterogeneities themselves upon loading. Overall, our model endothelial cells exhibited an increase in heterogeneity of basal cell strains when placed on the

representative aged matrix compared to the young matrix. Limitations of our study prohibit the extrapolation of these findings to alive cells, and future work should further examine how cells respond to micro-scale stiffness heterogeneities, which may impact cellular function and signaling.

Conflict of Interest: The authors declare that they have no conflict of interest.

References

Awolesi M, Widmann M, Sessa W, Sumpio B (1994) Cyclic strain increases endothelial nitric oxide synthase activity. Surgery 116:439–444 . doi: 10.1172/JCI118181

Barry AK, Wang N, Leckband DE (2015) Local VE-cadherin mechanotransduction triggers long-ranged remodeling of endothelial monolayers. J Cell Sci 128:1341–1351 . doi: 10.1242/jcs.159954

Birukov KG (2009) Cyclic stretch, reactive oxygen species, and vascular remodeling. Antioxid Redox Signal 11:1651–67 . doi: 10.1089/ars.2008.2390

Birukov KG, Bardy N, Lehoux S, et al (1998) Intraluminal pressure is essential for the maintenance of smooth muscle caldesmon and filamin content in aortic organ culture. Arterioscler Thromb Vasc Biol 18:922–927 . doi: 10.1161/01.atv.18.6.922

Breckenridge MT, Desai RA, Yang MT, et al (2014) Substrates with engineered step changes in rigidity induce traction force polarity and durotaxis. Cell Mol Bioeng 7:26–34 . doi: 10.1007/s12195-013-0307-6

Caille N, Tardy Y, Meister JJ (1998) Assessment of strain field in endothelial cells subjected to uniaxial deformation of their substrate. Ann Biomed Eng 26:409–416 . doi: 10.1114/1.132

Caille N, Thoumine O, Tardy Y, Meister J-J (2002) Contribution of the nucleus to the mechanical properties of endothelial cells. J Biomech 35:177–187 . doi: 10.1016/S0021-9290(01)00201-9

Civelekoglu G, Tardy Y, Meister JJ (1998) Modeling actin filament reorganization in endothelial cells subjected to cyclic stretch. Bull Math Biol 60:1017–1037 . doi: 10.1016/S0092-8240(98)90001-5

Cohen RA, Weisbrod RM, Gericke M, et al (1999) Mechanism of nitric oxide–induced vasodilatation. Circ Res 84:210–219 . doi: 10.1161/01.RES.84.2.210

Dan A, Huang RB, Leckband DE (2016) Dynamic Imaging Reveals Coordinate Effects of Cyclic Stretch and Substrate Stiffness on Endothelial Integrity. Ann Biomed Eng 1–13 . doi: 10.1007/s10439-016-1677-4

Du W, Mills I, Sumpio BE (1995) Cyclic strain causes heterogeneous induction of transcription factors, AP-1, CRE binding protein and NF-kB, in endothelial cells: Species and vascular bed diversity. J Biomech 28:1485–1491 . doi: 10.1016/0021-9290(95)00096-8

Ferko MC, Bhatnagar A, Garcia MB, Butler PJ (2007) Finite-element stress analysis of a multicomponent model of sheared and focally-adhered endothelial cells. Ann Biomed Eng 35:208–223 . doi: 10.1007/s10439-006-9223-4

Gilchrist CL, Witvoet-Braam SW, Guilak F, Setton LA (2007) Measurement of intracellular strain on deformable substrates with texture correlation. J Biomech 40:786–794 . doi: 10.1016/j.jbiomech.2006.03.013

Graham HK, Akhtar R, Kridiotis C, et al (2011) Localised micro-mechanical stiffening in the ageing aorta. Mech Ageing Dev 132:459–467 . doi: 10.1016/j.mad.2011.07.003

Helmke BP, Rosen AB, Davies PF (2003) Mapping mechanical strain of an endogenous cytoskeletal network in living endothelial cells. Biophys J 84:2691–2699 . doi: 10.1016/S0006-3495(03)75074-7

Huynh J, Nishimura N, Rana K, et al (2011) Age-related intimal stiffening enhances endothelial permeability and leukocyte transmigration. Sci Transl Med 3:112ra122 . doi: 10.1126/scitranslmed.3002761

Kohn JC, Chen A, Cheng S, et al (2016) Mechanical heterogeneities in the subendothelial matrix develop with age and decrease with exercise. J Biomech 49:1447–1453 . doi: 10.1016/j.jbiomech.2016.03.016

Kohn JC, Zhou DW, Bordeleau F, et al (2015) Cooperative effects of matrix stiffness and fluid shear stress on endothelial cell behavior. Biophys J 108:471–478 . doi: 10.1016/j.bpj.2014.12.023

Krishnan R, Klumpers DD, Park CY, et al (2011) Substrate stiffening promotes endothelial monolayer disruption through enhanced physical forces. Am J Physiol Cell Physiol 300:C146–C154 . doi: 10.1152/ajpcell.00195.2010

Kuebler WM, Uhlig U, Goldmann T, et al (2003) Stretch activates nitric oxide production in pulmonary vascular endothelial cells in situ. Am J Respir Crit Care Med 168:1391–1398 . doi: 10.1164/rccm.200304-562OC

Leung DY, Glagov S, Mathews MB (1976) Cyclic stretching stimulates synthesis of matrix components by arterial smooth muscle cells in vitro. Science (80-) 191:475–477 . doi: 10.1126/science.128820

Lo CM, Wang HB, Dembo M, Wang YL (2000) Cell movement is guided by the rigidity of the substrate. Biophys J 79:144–152 . doi: 10.1016/S0006-3495(00)76279-5

Lusis A (2000) Atherosclerosis. Nature 407:233–241 . doi: 10.1038/35025203.Atherosclerosis

Milner JS, Grol MW, Beaucage KL, et al (2012) Finite-element modeling of viscoelastic cells during high-frequency cyclic strain. J Funct Biomater 3:209–224 . doi: 10.3390/jfb3010209

Mullen CA, Vaughan TJ, Voisin MC, et al (2014) Cell morphology and focal adhesion location alters internal cell stress. J R Soc Interface 11:20140885–20140885 . doi: 10.1098/rsif.2014.0885

Nelson CM, Jean RP, Tan JL, et al (2005) Emergent patterns of growth controlled by multicellular form and mechanics. Proc Natl Acad Sci U S A 102:11594–11599 . doi: 10.1073/pnas.0502575102

Park JS, Chu JSF, Cheng C, et al (2004) Differential effects of equiaxial and uniaxial strain on mesenchymal stem cells. Biotechnol Bioeng 88:359–368 . doi: 10.1002/bit.20250

Reinhart-King CA, Dembo M, Hammer DA (2008) Cell-cell mechanical communication through compliant substrates. Biophys J 95:6044–6051 . doi: 10.1529/biophysj.107.127662

Schaffer JL, Rizen M, L'Italien GJ, et al (1994) Device for the application of a dynamic biaxially uniform and isotropic strain to a flexible cell culture membrane. J Orthop Res 12:709–719 . doi: 10.1002/jor.1100120514

Sinha R, Le Gac S, Verdonschot N, et al (2016) Endothelial cell alignment as a result of anisotropic strain and flow induced shear stress combinations. Sci Rep 6:29510 . doi: 10.1038/srep29510

Slomka N, Gefen A (2010) Confocal microscopy-based three-dimensional cell-specific modeling for large deformation analyses in cellular mechanics. J Biomech 43:1806–1816 . doi: 10.1016/j.jbiomech.2010.02.011

Trachet B, Fraga-Silva RA, Londono FJ, et al (2015) Performance comparison of ultrasound-based methods to assess aortic diameter and stiffness in normal and aneurysmal mice. PLoS One 10:e0129007 . doi: 10.1371/journal.pone.0129007

Valent ET, van Nieuw Amerongen GP, van Hinsbergh VWM, Hordijk PL (2016) Traction force dynamics predict gap formation in activated endothelium. Exp Cell Res 347:161–170 . doi: 10.1016/j.yexcr.2016.07.029

Von Offenberg Sweeney N, Cummins PM, Birney YA, et al (2004) Cyclic strain-mediated regulation of endothelial matrix metalloproteinase-2 expression and activity. Cardiovasc Res 63:625–634 . doi: 10.1016/j.cardiores.2004.05.008

Weisstein EW Full Width at Half Maximum. In: MathWorld--A Wolfram Web Resour. http://mathworld.wolfram.com/FullWidthatHalfMaximum.html. Accessed 21 Apr 2017

Yao Y, Lacroix D, Mak AFT (2016) Effects of oxidative stress-induced changes in the actin cytoskeletal structure on myoblast damage under compressive stress: confocal-based cell-specific finite element analysis. Biomech Model Mechanobiol 15:1–14 . doi: 10.1007/s10237-016-0779-0

Figures

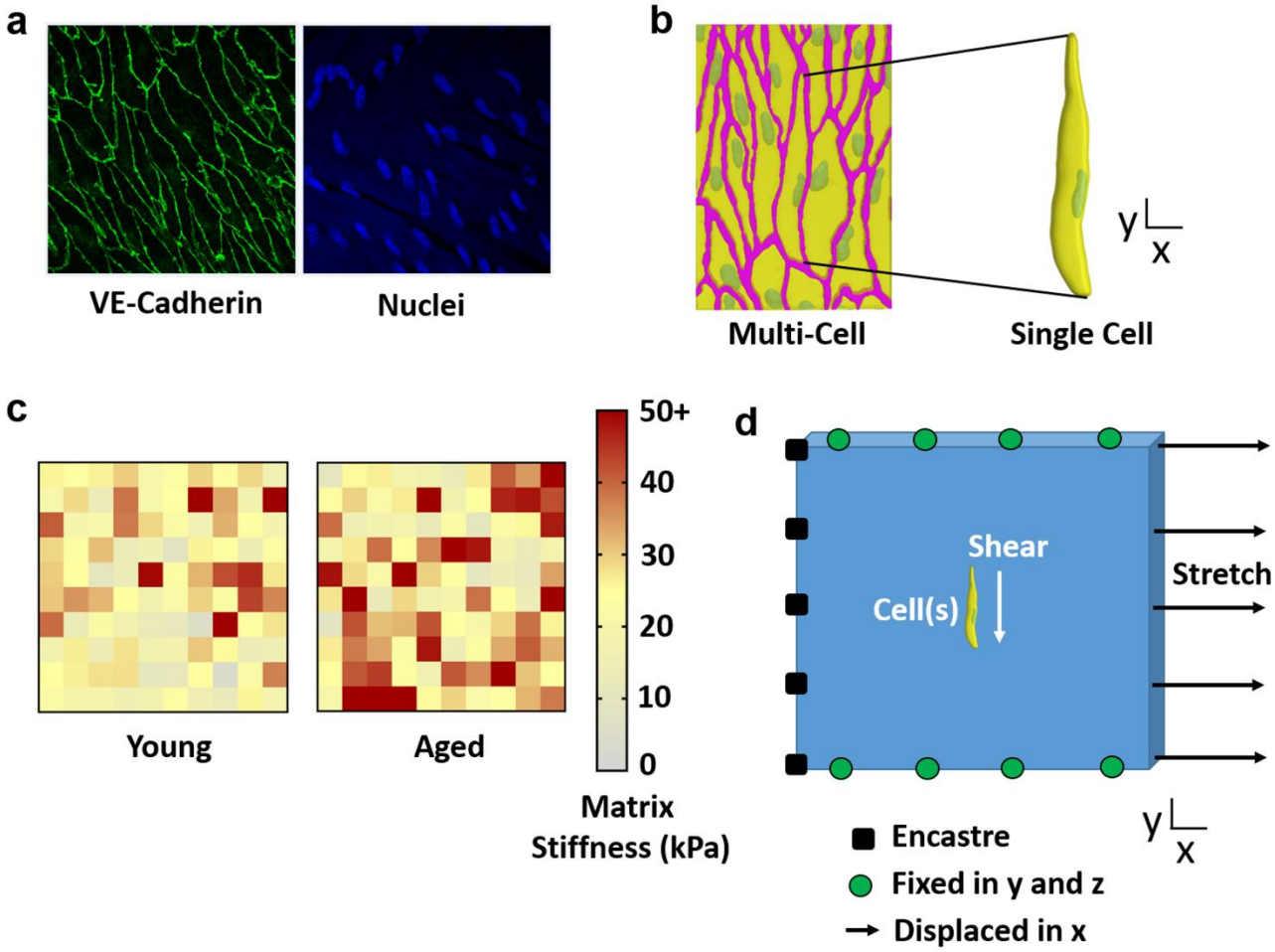

Figure 1

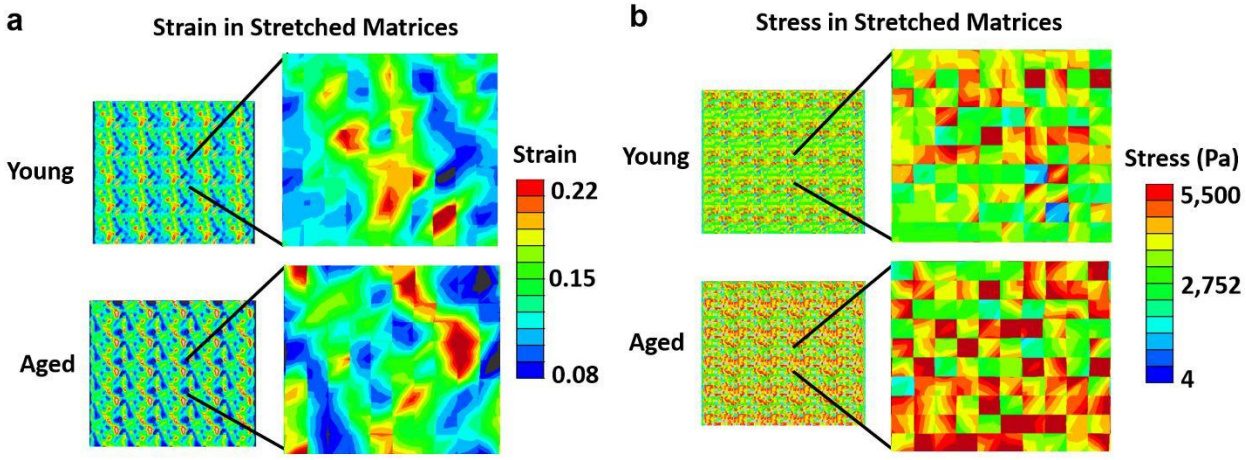

Figure 2

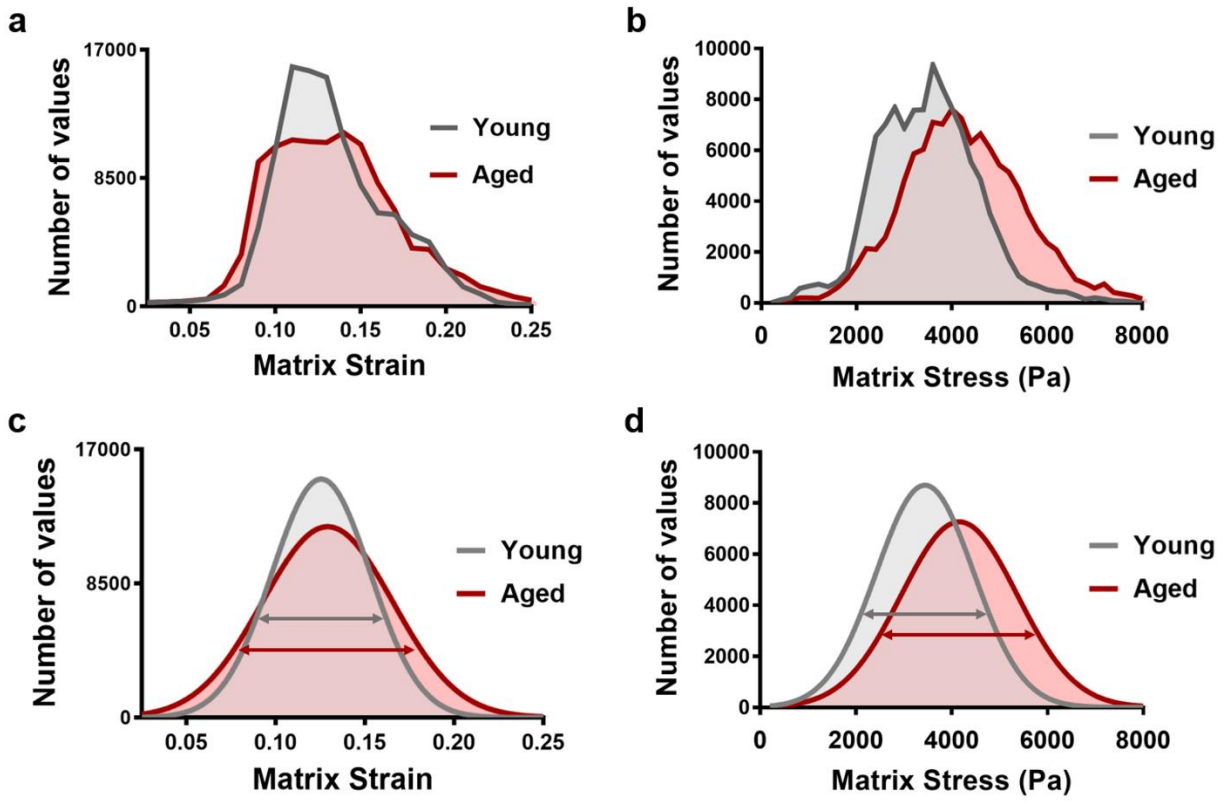

Figure 3

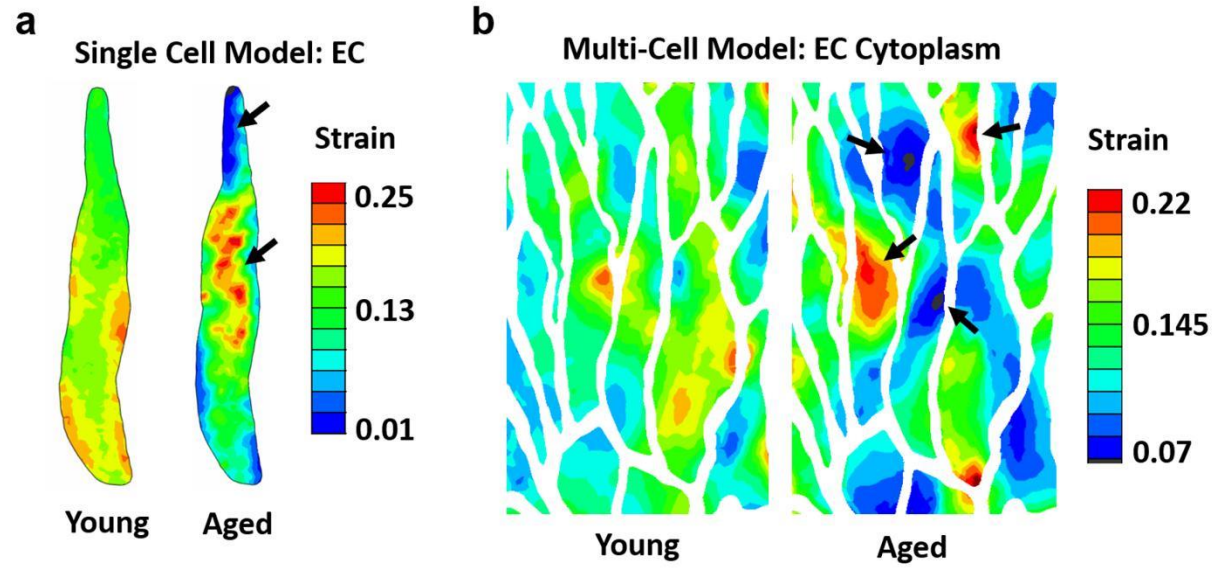

Figure 4

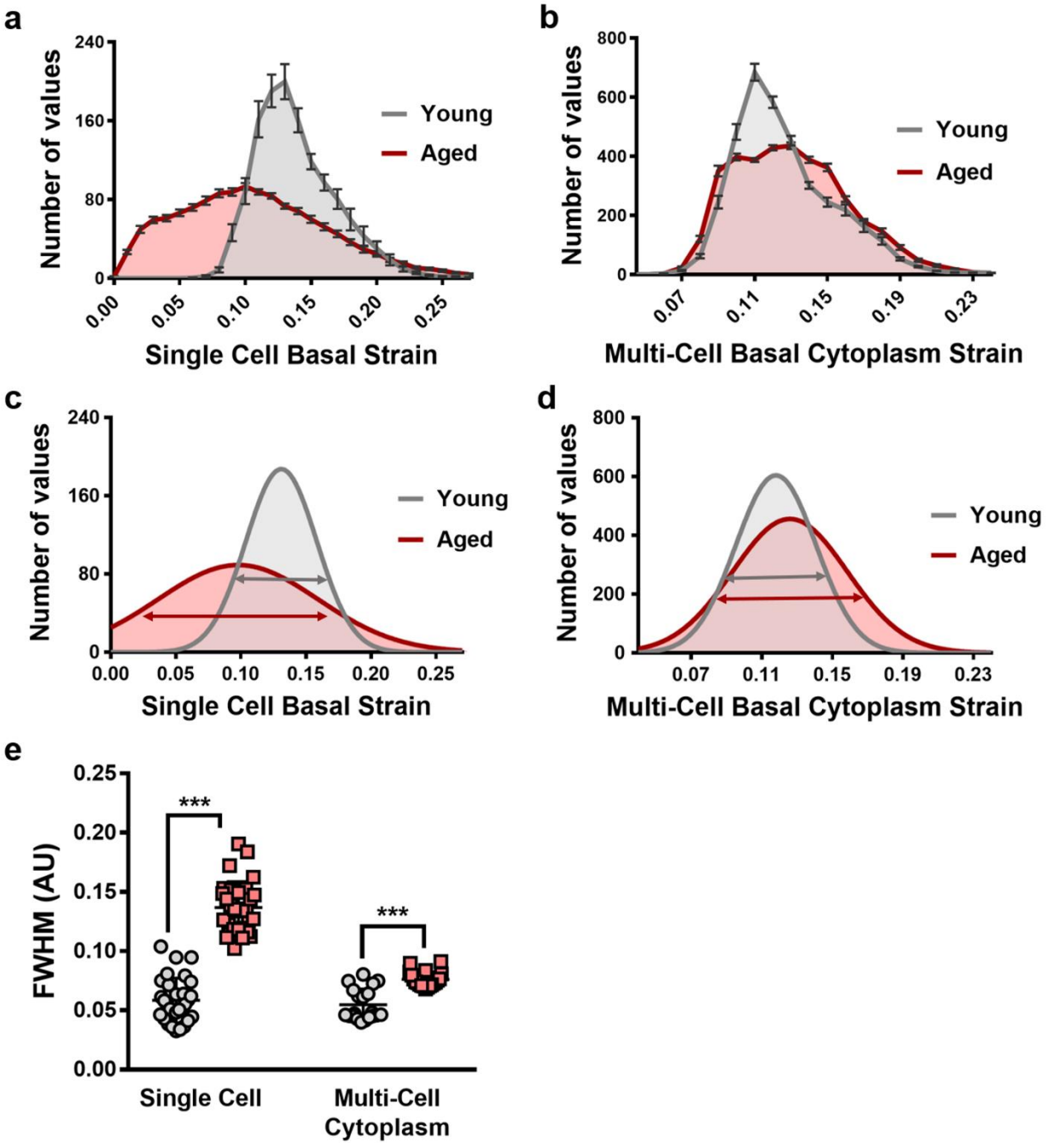
a
Number of values
240
160
80
0
Young
Aged
0.00
0.05
0.10
0.15
0.20
0.25
Single Cell Basal Strain
b
Number of values
800
600
400
200
0
Young
Aged
0.07
0.11
0.15
0.19
0.23
Multi-Cell Basal Cytoplasm Strain
c
Number of values
240
160
80
0
Young
Aged
0.00
0.05
0.10
0.15
0.20
0.25
Single Cell Basal Strain
d
Number of values
800
600
400
200
0
Young
Aged
0.07
0.11
0.15
0.19
0.23
Multi-Cell Basal Cytoplasm Strain
e
FWHM (AU)
0.25
0.20
0.15
0.10
0.05
0.00
***
***
Single Cell
Multi-Cell
Cytoplasm

Figure 5

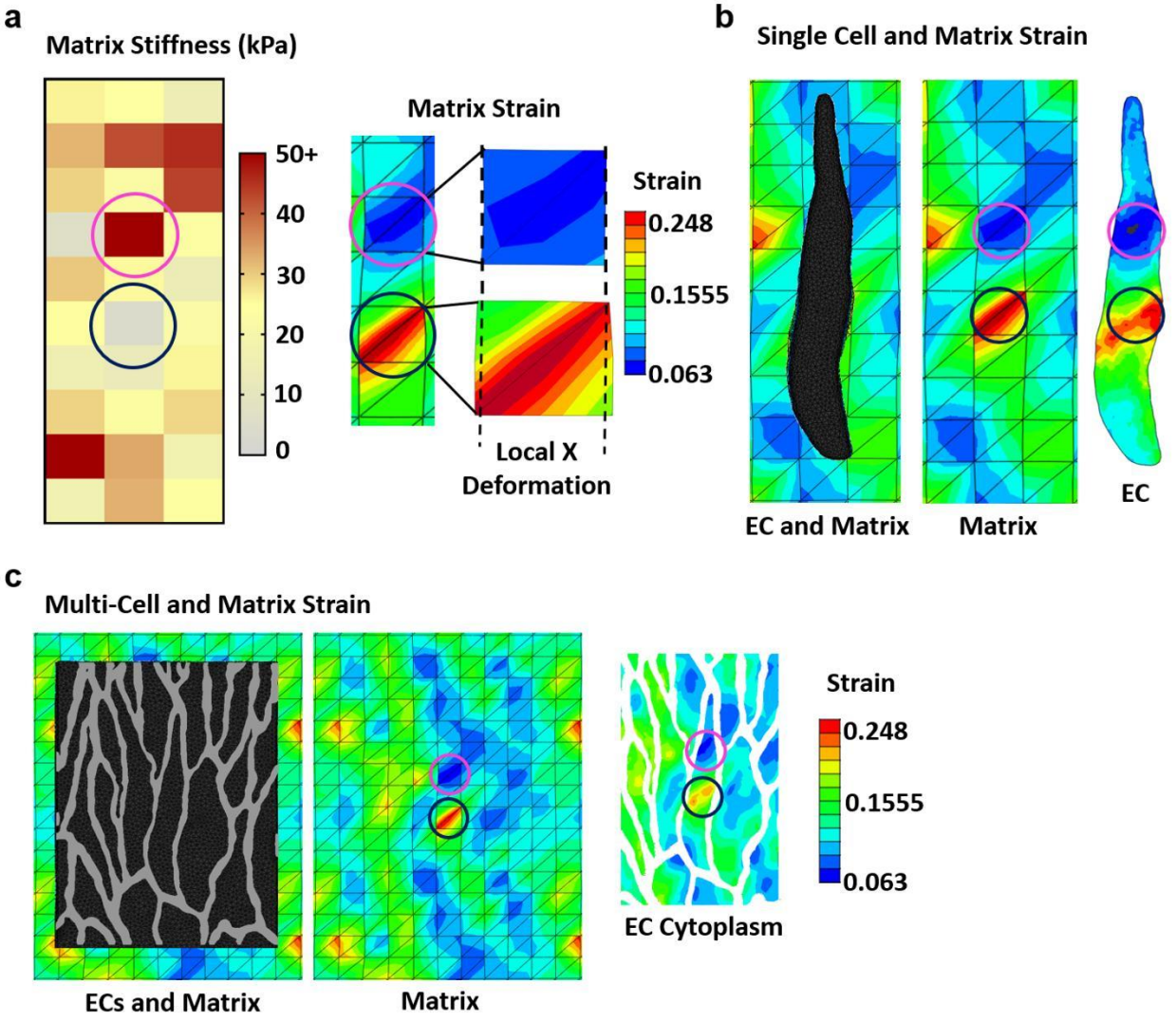

Figure 6

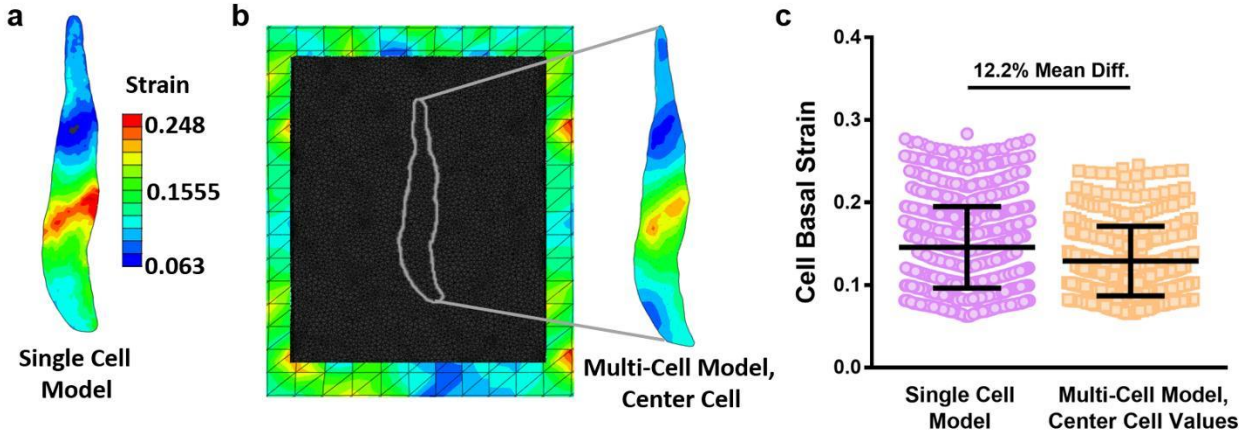

Figure 7